Hindawi
Advances in Civil Engineering
Volume 2024, Article ID 3076780, 10 pages
https://doi.org/10.1155/2024/3076780

Research Article

Study on Acoustic Emission Characteristics and Damage Evolution Law of Shale under Uniaxial Compression

Wenjie Wu,[1,2] **Chee-Ming Chan**,[1] **Yilei Gu**,[3] **and Xiaopeng Su**[4]

[1] *Faculty of Engineering Technology, Universiti Tun Hussein Onn Malaysia, Parit Raja 86400, Johor, Malaysia*
[2] *Information Engineering, Fujian Forestry Vocational and Technical College, Nanping 353000, China*
[3] *State Key Laboratory of Coal Mine Disaster Dynamics and Control, Chongqing University, Chongqing 400044, China*
[4] *School of Civil Engineering, Chongqing Jiaotong University, Chongqing 400074, China*

Correspondence should be addressed to Wenjie Wu; hn210005@student.uthm.edu.my

Received 27 July 2023; Revised 16 January 2024; Accepted 29 January 2024; Published 13 February 2024

Academic Editor: Robert Černý

Investigating the correlation between acoustic emission (AE) parameters and damage mechanisms in rock mechanics can help understand rock damage evolution under loading and provide a theoretical basis for engineering support and safety detection. Therefore, this paper presents experimental works on the correlation between AE and failure mechanisms of rock mass under uniaxial compression stress, with the aim of capturing the damage evolution leading to a new damage constitutive model. The experimental results indicate that the uniaxial compression process of shale can be divided into four stages according to AE characteristics. AE signals are minimal during the crack compaction and elastic stages. The crack initiation strength σ_{ci}, which is approximately 55% of the uniaxial compressive strength, is identified when the cumulative AE counts and damage factor begin to increase slowly. When axial stress reaches the damage strength σ_{cd}, which is approximately 80% of the uniaxial compressive strength, a significant number of AE signals are generated. AE phenomena can be observed during the unstable crack development and post-crack stages. Considering the initial damage to the rock, the damage factor D initially decreases and then increases with increasing cumulative ring-down counts rather than exhibiting a monotonic increase. The damage factor D is proportional to the cumulative AE counts N in the stage before rock failure.

1. Introduction

The emergence, propagation, intersection, and permeation of microcracks noticeably impact the mechanical characteristics of rock mass. The behavior of these microcracks is complex. Damage mechanics is always used for the study of the mechanical processes and damage evolution until failure during deformation [1]. Many scholars used different parameters to study the rock damage process, such as the number of rock cracks [2–3], strain [4–6], energy evolution [7], and acoustic emission (AE) signal parameters [6–8].

AE technique is a developed nondestructive testing method, which has proved to be a reliable tool for many types of studies [9–10]. Figure 1 shows some characteristic parameters of a simplified AE signal, including rise time, duration time, AE count, and maximum amplitude, and these AE parameters can be used to evaluate the damage severity and identify the nature of damage directly or indirectly [11]. The pattern recognition proposed by Thirumalaiselvi and Sasmal [12] based on AE methods would be very effective in monitoring the state of in-service structures where the health information of the structure can be automatically and continuously assessed through the emitted acoustic signals from microcrack formation. The AE technique was also used as a passive nondestructive tool to detect the damage progress in short glass fiber-reinforced composite panels [13]. De Smedt et al. [14] also used AE damage monitoring to better understand the (cyclic) uniaxial tensile behavior of steel fiber-reinforced concretes. Livadiotis et al. [15] monitored the corrosion of steel pipelines using the AE technique. Andraju and Raju [16] employed used AE and digital image correlation techniques to describe the evolution of intra/interlaminar damage modes in the carbon fiber-reinforced plastics laminates under in-plane/out-of-plane loading conditions.

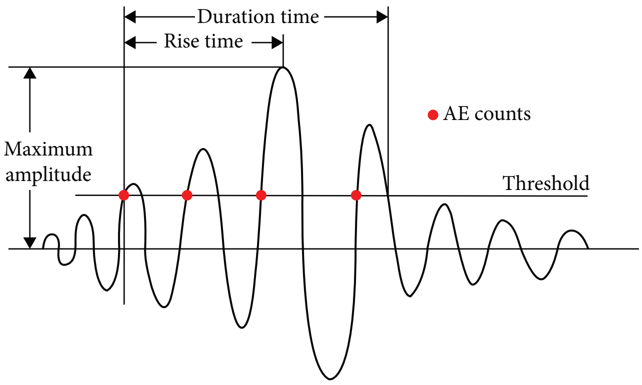

Figure 1: Characteristic parameters of a simplified AE hit [11].

When solid materials such as rocks are subjected to an external load or temperature, their internal defects cause cracking of materials or structures, resulting in damage and destruction. In the process of damage and destruction, the strain energy is released in the form of an elastic wave, which spreads rapidly in solid materials such as rock mass, resulting in the phenomenon of AE [17]. AE information can reflect the evolution law of rock damage [18]. With the help of AE characteristics, it is of great significance to understand the failure mechanism and damage evolution of rock. Therefore, the AE technique has also been widely used to investigate crack propagation, source location, and damage quantification in rocks and other solid materials [9, 17–22]. Shkuratnik et al. [23] studied the memory effect of coal specimens in complex stress processes by performing triaxial cyclic loading and unloading experiments. Liu et al. [24] analyzed AE characteristics of coal rock under uniaxial compression and proposed a new damage factor, which was defined based on the normalized cumulative ring-down count of AE. The damage model of coal rock under uniaxial compression was established based on this factor, and they thought that the damage increased monotonically with the AE signal [24]. Moradian et al. [25] pointed out that AE has enough accuracy to monitor the shear behavior of the joints, and it could be used in-site confidently. Yang et al. [26] carried out AE experiments under triaxial compression, analyzed the characteristics of limestone damage evolution through AE parameters, and concluded that the damage factor increased monotonously. Yu et al. [27] carried out AE experiments on coal rock under different confining stresses to reveal the change rule of the ring-down counts rate, the temporal and spatial distribution of AE, b value of AE, and damage characteristics and to provide a theoretical basis for prediction of coal–rock damage. Recently, different artificial intelligence (AI) methods have been applied to various aspects of rock mechanics and civil engineering, owing to its ability to handle complex problems [28, 29]. A study showed that the prefailure AE indeed encapsulates information about the developing failure mechanisms and the post-failure response in rocks, which can be captured through AI [10].

However, while there are numerous studies that rely on AE parameters to investigate rock damage, there still remains a paucity of quantitative studies. To further investigate the relationship between AE parameters and rock failure mechanisms, as well as to better elucidate the law governing the evolution of rock damage, this paper aims to conduct AE experiments on shale under uniaxial compression. The AE characteristics and the damage evolution process were analyzed, and a damage constitutive model based on AE characteristics was established.

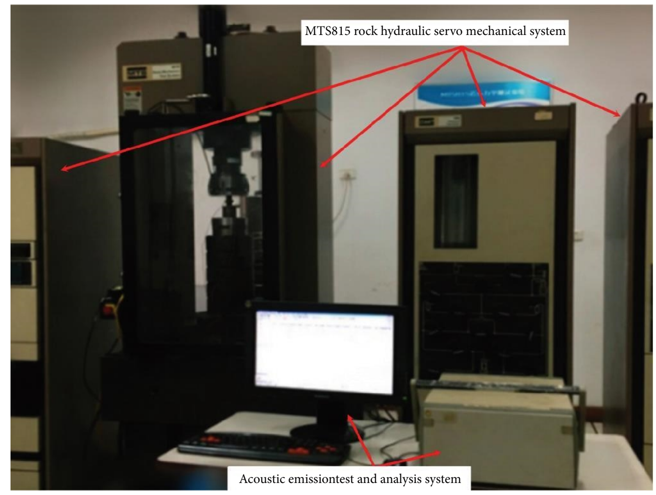

Figure 2: Experimental instrument.

2. Experimental Materials, Apparatus, and Methods

2.1. Preparation of Rock Specimen. The shale used in this study was taken from argillaceous shales of the Silurian Luojiaping Formation in the Pengshui area, Chongqing, with clear bedding and crack distribution. The rock blocks that met the experimental requirements were selected. Rock sampling was performed in the laboratory of Chongqing University. All specimens were processed into standard cylinders with dimensions of Φ 50 mm × 100 mm, following the International Society of Rock Mechanics standard [30]. To ensure the relative consistency of the properties of specimens, all the specimens were obtained from the same rock block and were taken along the bedding direction. Due to the swelling and disintegration of the rock specimens because of water, anhydrous polishing was used during the rock specimen production process.

2.2. Experimental Instrument. MTS815 rock hydraulic servo mechanical system and the PCI-II AE test and analysis system produced by the American acoustic physics company Physical Acoustic Corporation were used as the testing system, as shown in Figure 2.

2.3. Experimental Procedure. During the experiments, it was important to maintain synchronization between the loading process and the monitoring of AE signals. AE signals were collected during the uniaxial compressive process. A layer of butter was applied between the AE sensors and the rock specimen, and a rubber band was used to secure the AE sensors tightly attached to the rock specimen, as shown in

Figure 3: Rock specimen and layout of AE sensors.

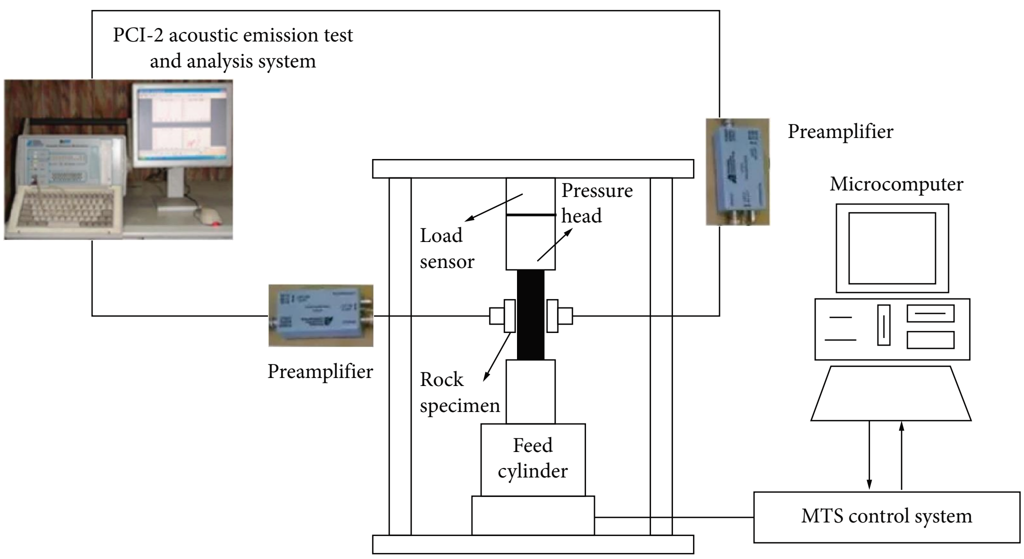

Figure 4: The schematic diagram of the experimental system.

Figure 3. The axial displacement loading method was adopted in the experiments, with a loading rate of 0.008 mm/min. The axial load was applied until the rock specimen failure, and the experiment ended. During the experiments, time, stress, strain, and AE signals were recorded synchronously.

The schematic diagram of the experimental system is shown in Figure 4. In Figure 4, the MTS control system controls the application of axial stress to the rock, and the PCI-2 AE test and analysis system mainly monitors and collects AE signals during uniaxial compression experiments. When a force is applied to a rock specimen, it will emit AE signals due to deformation or crack, and elastic waves emitted from the AE source propagate from inside the rock specimen to the surface of the rock specimen and cause mechanical vibration on the surface. AE sensors attached to the surface of the rock specimen convert the transient displacement caused by mechanical vibration into electrical signals. The received acoustic transmission signals were then amplified and processed by the preamplifier. Its characteristic parameters are formed, which are recorded and displayed on the computer. It should be noted that the threshold of AE was set to 30 dB based on AE threshold pretesting, and it was found that when the threshold was set to 30 dB, the AE instrument did not receive any external signals, thereby eliminating the interference of external signals in this experiment.

3. Results and Discussion

3.1. Mechanical Properties of Shale under Uniaxial Compression. Using the experiment method mentioned above, the stress–strain curves of the shale specimens under uniaxial conditions are obtained, as shown in Figure 5. The mechanical parameters (Table 1) and the stress–strain curves (Figure 5) indicate that the compressive strength of the shale specimens drilled along the

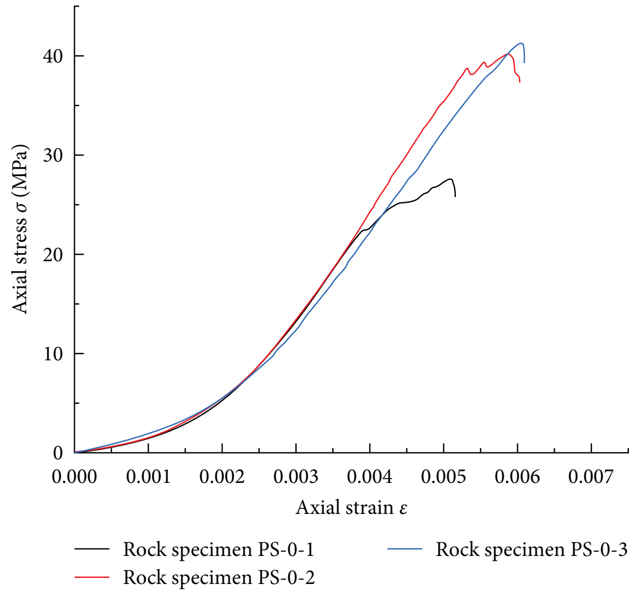

Figure 5: Stress–strain curve of shale under uniaxial compression.

Table 1: Mechanical parameters under uniaxial compression of shale.

Specimen number	Diameter (cm)	Length (cm)	Sampling direction (-)	Compressive strength (MPa)	Peak axial strain (%)	Poisson's ratio (-)
PS-0-1	48.92	99.46	Parallel bedding	27.51	0.51	
PS-0-2	48.9	99.08	Parallel bedding	40.13	0.59	0.28
PS-0-3	48.92	99.09	Parallel bedding	41.24	0.61	

direction parallel to the bedding direction has some degree of dispersion, with an average value of 36.29 MPa. The uniaxial compressive strength of shale is positively correlated with the peak axial strain. The stress–strain curves exhibit large fluctuations, particularly in the unstable crack development stage of shale, where it shows an obvious zigzag shape, mainly because shale broke and slipped mainly along the bedding plane. The stress–strain curves also exhibit the phenomenon of stress drop before reaching peak strength. This drop mainly results from the fact that, after the support point of the failure surface was damaged, the local stress dropped in a short time before reaching the next support point.

3.2. Analysis of AE Characteristics of Shale under Uniaxial Compression. The AE amplitude and cumulative ring-down counts obtained in these experiments reflected the AE phenomenon of shale with consistent patterns. Due to article length limitations, this paper analyzed the relationship between AE amplitude, cumulative ring-down counts, stress, and time in the failure process of rock specimens PS-0-1 and PS-0-2, as shown in Figures 6 and 7. From Figures 6 and 7, it can be concluded that the AE characteristics of various stages during the deformation and failure process of shale have the following general rules.

(1) *Crack compaction stage*. Under axial compression, the original open structural plane or microcrack in the specimen gradually closes, leading to nonlinear deformation, with a concave shape in the stress–strain curve. At this stage, there are less AE activity and lower AE energy. The slope of the cumulative ring-down counts curve increases very slowly.

(2) *From the elastic stage to the stable development stage of microelastic cracks*. The stress–strain curve is approximately linear at this stage. In the elastic deformation stage, there is no AE phenomenon. However, when the axial stress continues to increase, there will be some AE events, indicating that the specimen is steadily growing. At this stage, the AE energy is basically undetectable, and the cumulative ring-down counts curve tends to flatten out.

(3) *Unstable crack development stage*. As axial stress continues to increase, the interaction between internal cracks of the specimen intensifies. The microcracks converge and coalesce, and AE events become active. The AE energy increases significantly compared to the previous stages, indicating that the rock specimen has entered the yield stage. The slope of the cumulative ring-down counts curve begins to increase slowly, and the stress corresponding to the turning point of the curve slope is the damage strength σ_{cd}, which is about 80% of the peak strength. As shown in Figure 6, the slope of the cumulative ring-down counts–time curve of rock specimen PS-0-1 starts to change at 232.8 s, and its corresponding stress value is 22.27 MPa, about 81% of the peak intensity.

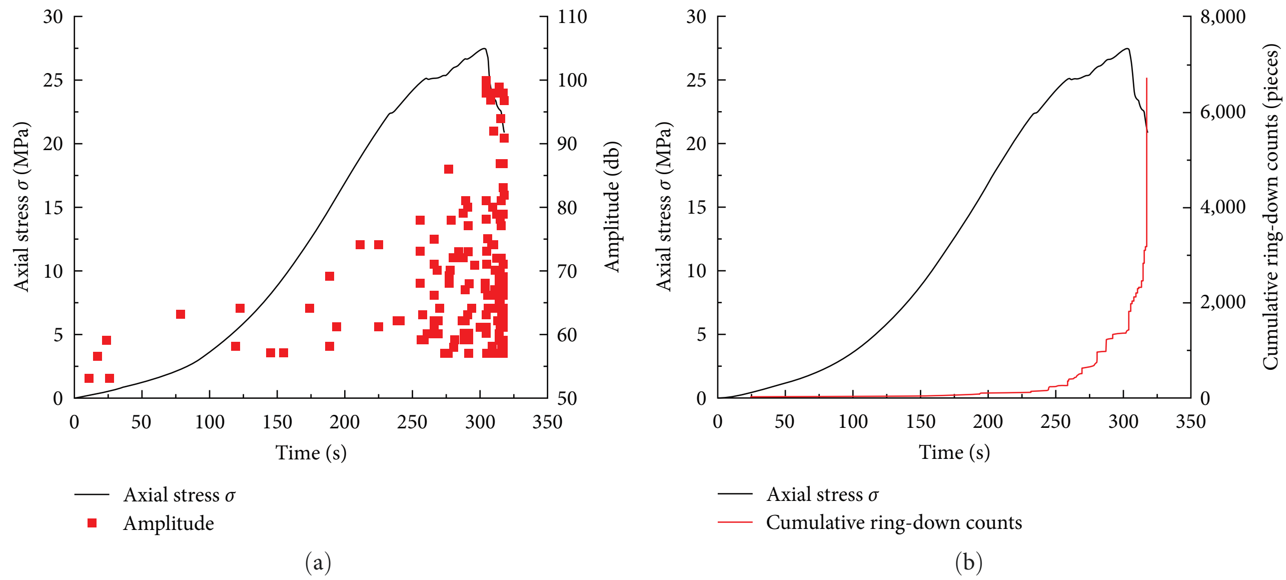

Figure 6: The relationship between AE parameters, stress and time of rock specimen PS-0-1 during the uniaxial compression process: (a) plot of amplitude and stress versus time; (b) plot of cumulative ring-down counts and stress versus time.

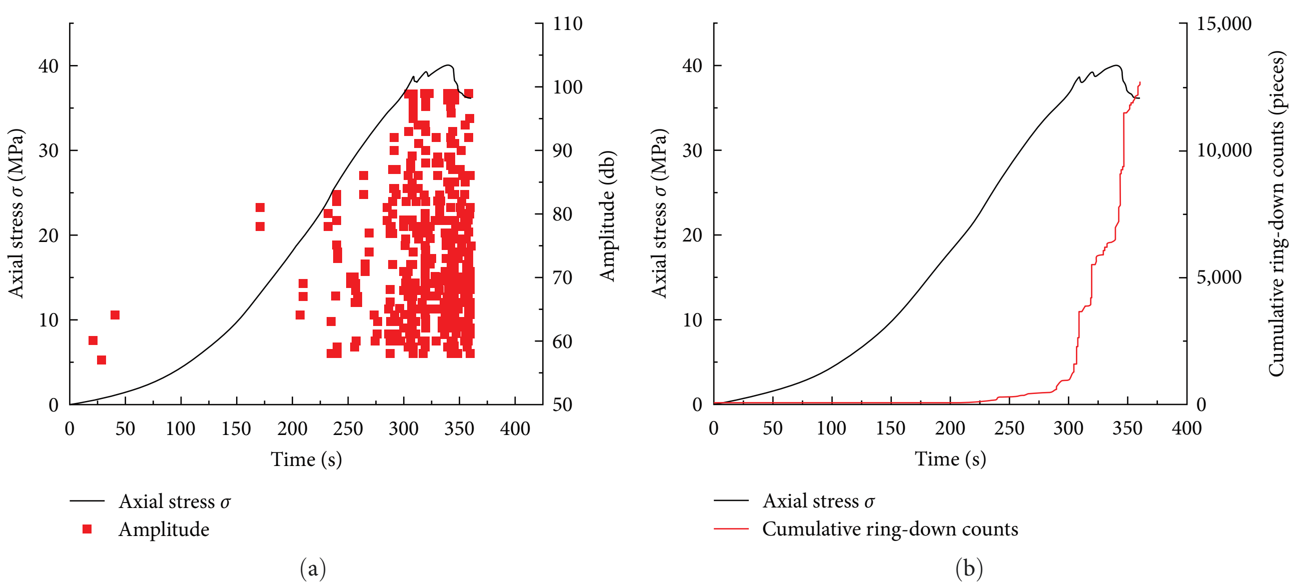

Figure 7: The relationship between AE parameters, stress and time of rock specimen PS-0-2 during the uniaxial compression process: (a) plot of amplitude and stress versus time; (b) plot of cumulative ring-down counts and stress versus time.

Additionally, the cumulative ring-down counts curve shows a step-like rise before the rock specimen failure.

(4) *Postfailure stage*. After the axial stress reaches the peak strength of the rock specimen, the internal structure of the specimen is damaged, and a macrocrack surface is formed. However, the specimen basically remains monolithic. The strength decreases rapidly with deformation, accompanied by a relatively strong AE phenomenon. The cumulative ring-down counts curve rises rapidly. This rise mainly results from the fact that, after the peak strength, the specimen slides along the macrocrack surface to produce a large number of AE signals. Compared with the AE of specimen PS-0-1, the AE energy of PS-0-2 is substantially higher. The primary reason is that when an external load is applied to the rock specimen, the greater the compressive strength of the rock specimen, the greater the energy stored in the specimen. At the moment of specimen failure, a large amount of energy is released, resulting in strong AE signals.

3.3. Characteristics of Damage in Shale under Uniaxial Compression. In 1963, Rabotnov, a former Soviet scholar, put forward the concept of damage factor. Lemaitre [31] of France proposed the strain equivalence-based hypothesis on

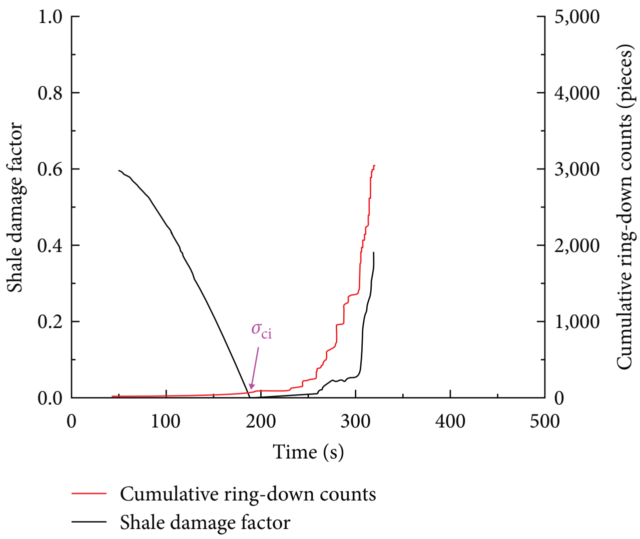

FIGURE 8: The relationship between shale damage factor and cumulative ring-down counts of rock specimen PS-0-1 and time.

this basis. According to his hypothesis, the basic relation of rock damage constitutive equation was established by assuming that rock elements obey the generalized Hooke law before failure.

$$\sigma = \sigma^* (1 - D) = E\varepsilon (1 - D), \tag{1}$$

where σ is apparent stress tensor, σ^* is effective stress tensor, D is damage factor, E is elastic modulus, ε is axial strain.

Numerous research findings revealed that cumulative ring-down count is a significant parameter that could effectively reflect the variation of material damage characteristics [32]. Therefore, in this paper, cumulative ring-down count was used as the characteristic parameter, and specimen PS-0-1 was selected as the analytical object to examine the damage evolution characteristics of shale.

3.3.1. Analysis of Shale Damage Characteristics under Uniaxial Compression. Based on the stress–strain curve obtained from the rock specimen PS-0-1 experiment, the elastic modulus E is 5,748 MPa. Using the stress–strain relationship obtained from the same experiment, the damage factor D is acquired using the formula $\sigma = \sigma^*(1 - D) = E\varepsilon (1 - D)$. Figure 8 shows the variation of damage factor D and cumulative ring-down counts N over time. Figure 8 shows that the damage factor D initially decreases and then increases. The reason why the damage factor D decreases first is due to the initial damage inside the rock specimen. The shale specimen may undergo various internal and external mechanical and geological actions, such as tectonic deformation, weathering, and unloading, which ultimately lead to internal damage. In addition, the process of drilling and grinding to make rock specimens also causes some damage to the specimens. These facts cause the rock to exhibit initial damage characteristics during the initial stages of uniaxial compression. During the crack compaction stage, the microcracks in the specimen gradually close, leading to an increase in rock strength and a decrease in damage. As a result, the damage factor D shows an initial decrease. As the axial stress continues to increase, cracks inside the specimen start to grow and connect gradually, leading to an increase in rock damage.

When cumulative ring-down counts and damage factor begin to slowly increase, it indicates that internal cracks in the specimen start to generate and expand. At this point, the corresponding stress is considered the crack initiation strength σ_{ci}, which is approximately 55% of the uniaxial compressive strength. For instance, the rock specimen PS-0-1 has a σ_{ci} of 15.1 MPa, which is approximately 54.9% of the peak strength, while the rock specimen PS-0-2 has a σ_{ci} of 23.5 MPa, which is about 58.6% of the peak strength.

3.3.2. Establishment of Damage Model Based on AE Characteristics for Shale under Uniaxial Compression. The former Soviet scholar Kachanov [33] defined the damage factor as follows:

$$D = \frac{A_d}{A}, \tag{2}$$

where A_d is the fault area where the rock specimen is damaged, including compaction, new crack generation, propagation, convergence, penetration, and macrofailure. A is the crack area at the initial nondestructive injury.

Assuming that cumulative ring-down counts of complete destruction of whole section A of the nondestructive material is N_c, then the ring-down counts N_w when the unit area element is destroyed as follows:

$$N_w = \frac{N_c}{A}. \tag{3}$$

When the damaged area reaches A_d, cumulative ring-down counts N_d is as follows:

$$N_w = N_w A_d = \frac{N_c A_d}{A}. \tag{4}$$

So

$$D = \frac{N_d}{N_c}. \tag{5}$$

During the experiment, due to insufficient stiffness of the testing machine or different crack conditions of rock specimens, the testing machine often stops working before the rock is destroyed (that is, the damage of rock specimens does not reach 1), so the damage factor is corrected as follows:

$$D = D_U \frac{N_d}{N_c}, \tag{6}$$

where D_U is the critical value of damage.

In Equation (6), the value of N_c is cumulative ring-down counts of the whole process of rock specimen compression failure, and the value of N_d is cumulative ring-down counts of each stage in the progress of rock specimen compression failure. To simplify the calculation, Liu et al. [24] normalized the damage critical value according to the method of linear function conversion, and Equation (7) was obtained.

$$D_U = 1 - \frac{\sigma_c}{\sigma_p}, \tag{7}$$

where σ_p is the peak strength and σ_c is the residual strength.

The damage model of coal rock under uniaxial compression, based on AE characteristics, can be expressed as follows:

$$\sigma = E\varepsilon(1 - D) = E\varepsilon\left(1 - D_U \frac{N_d}{N_c}\right). \tag{8}$$

From the above equation, it can be observed that the damage factor D is directly proportional to cumulative ring-down counts N when the specimen is undamaged. The damage factor D increases with an increase in the cumulative ring-down counts N.

However, the rock specimens utilized in this experiment exhibited a certain degree of initial damage. Existing rock material damage models have generally overlooked the initial damage characteristics of rock materials, despite the presence of such characteristics in actual rock materials [34]. Similar to the aforementioned method, a damage constitutive model for shale under uniaxial compression based on AE characteristics is established as follows:

$$\begin{cases} \sigma = E\varepsilon(1 - D) \\ D = -K_1 \dfrac{N_0 - N_d}{N_c}, & 0 \le N_d \le N_0 \\ D = K_2 \times \dfrac{N_d - N_0}{N_c}, & N_c \ge N_d \ge N_0 \end{cases}, \tag{9}$$

where σ is principal stress, ε is axial strain, K_1 and K_2 are damage evaluation index, and N_0 is the cumulative ring-down counts when the damage factor is 0.

Using Origin software, damage factor value D and cumulative ring-down counts value N are marked on the coordinate axis during the experiment, and the relationship between the two objects is obtained by linear fitting. As shown in Figure 8, the damage factor D exhibits a decreasing-then-increasing trend with an increase in cumulative ring-down counts N. The relationship between damage factor D and cumulative ring-down counts N is obtained via linear fitting of the two segments. Alternatively, cumulative ring-down counts value N and corresponding damage value D obtained during the experiment (18, 0.46), (66, 0), (3,020, 0.33) are substituted into Equation (9). This approach leads to the development of a damage constitutive model for rock specimen PS-0-1 as follows:

$$\begin{cases} \sigma = E\varepsilon(1 - D) \\ D = -9.7 \times 10^{-3} N + 0.64, & 0 \le N < 66 \\ D = 0.334 \dfrac{N - 66}{3,020}, & N \ge 66 \end{cases}. \tag{10}$$

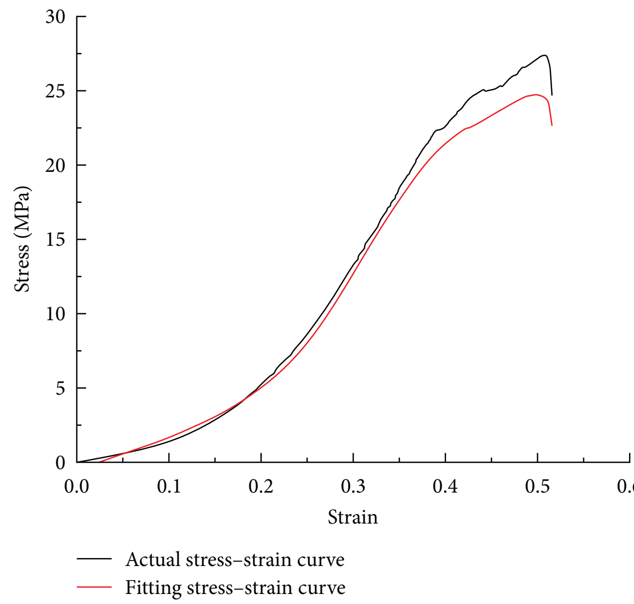

Figure 9: Comparison between theoretical and experimental stress–strain curve of rock specimen PS-0-1.

3.3.3. Comparative Analysis of Theoretical Stress–Strain Curve and Experimental Curve. Using Origin software, the theoretical stress–strain curve obtained based on the damage constitutive model of rock specimen PS-0-1 is compared with the actual stress–strain curve obtained from the experiment, as illustrated in Figure 9. The comparison shows good agreement between the two curves. The relationship between damage factor D and cumulative ring-down counts N for rock specimen PS-0-2 is obtained using linear fitting with Origin software in four stages, ensuring that the coefficient of determination R^2 was close to 1 (Crack compaction stage, $R^2 = 0.85387$. From the elastic stage to the stable development stage of the microelastic crack, $R^2 = 0.92259$. Unstable crack development stage, $R^2 = 0.87494$. Postfailure stage, $R^2 = 0.73169$). This process leads to the development of a damage constitutive model for rock specimen PS-0-2. Finally, the theoretical stress–strain curve obtained from the damage constitutive model of rock specimen PS-0-2 is compared with the actual stress–strain curve obtained from the experiment, as presented in Figure 10. The comparison shows a perfect agreement between the two curves, which proves the rationality of the developed damage constitutive model.

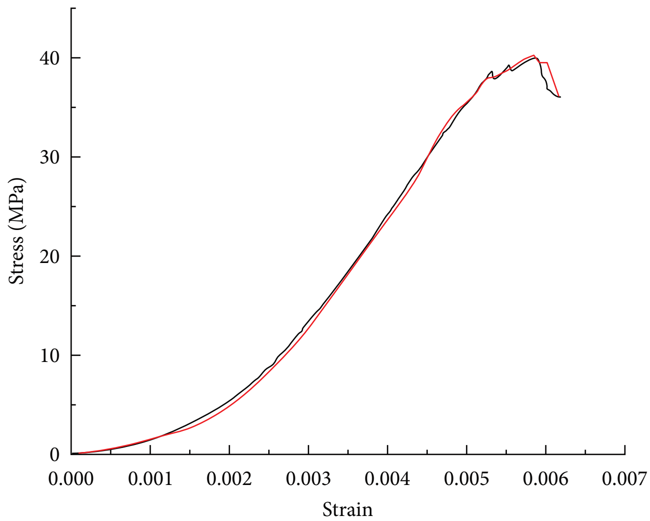

Figure 10: Comparison between theoretical and experimental stress–strain curve of rock specimen PS-0-2.

4. Conclusions

This paper investigated the AE law and damage evolution characteristics of shale under uniaxial compression conditions and established a uniaxial compression damage constitutive model of shale based on AE characteristics. The conclusions are as follows:

(1) The compressive strength of shale specimens drilled parallel to the bedding direction exhibits a certain degree of dispersion. The stress–strain curve of shale under uniaxial compression obtained in this experiment displays some fluctuations, particularly during the stage of unstable crack development, with an evident zigzag pattern.

(2) The uniaxial compression process of shale is divided into four stages according to the characteristics of AE. The crack initiation strength σ_{ci}, which is approximately 55% of the peak strength, is identified when the cumulative AE counts and damage factor begin to increase slowly. When the axial stress reaches the damage strength σ_{cd}, which is approximately 80% of the peak strength, a significant number of AE signals start to be generated. The cumulative ring-down counts curve of AE exhibits a stepwise increase prior to the failure of the rock specimen.

(3) Considering the initial damage of the rock, the damage factor D demonstrates a decreasing-then-increasing trend with an increase in the cumulative ring-down counts rather than exhibiting a monotonic increase. This helps to further understand the internal damage evolution mechanism of rocks.

(4) By analyzing the AE characteristics of shale at different stages, a relationship between damage factor D and cumulative ring-down counts N at various stages is obtained via linear fitting with origin software. This approach enables the establishment of a more reasonable shale damage constitutive model, thereby resulting in a theoretical stress–strain curve that is consistent with the actual stress–strain curve. It is worth noting that in the AE experiment of the whole process of uniaxial compression experiment, the damage factor D is proportional to cumulative ring-down counts N only in the stage before the peak strength of the rock, not the whole process. Therefore, it is necessary to conduct research on the relationship between rock damage and AE parameters after rock failure in the future to establish a postpeak rock damage model based on AE characteristics.

Symbols

σ: Apparent stress tensor
σ^*: Effective stress tensor
σ_{ci}: Crack initiation strength
E: Elastic modulus
ε: Axial strain
K_1/K_2: Damage evaluation index
A_d: The fault area where the rock specimen is damaged
N_c: Cumulative ring-down counts when the experiment is over
N_d: Cumulative ring-down counts when damage area reaches A_d
σ_p: Peak strength
σ_c: Residual strength
σ_{cd}: Damage strength
D_U: Critical value of damage
D: Damage factor
R: Coefficient of determination, indicating goodness of fit
A: The crack area at the initial nondestructive injury
N_w: Ring-down counts when the unit area element is destroyed
N_0: Cumulative ring-down counts when the damage factor is 0.

Data Availability

The proposed model and data used during the current study are available from the corresponding author.

Consent

Written informed consent for publication of this paper was obtained from the affiliated institutions and all authors.

Disclosure

This present study is a part of the PhD thesis of author Wenjie Wu. The experiment was conducted in the State Key Laboratory of the College of Resources and Environmental Engineering, Chongqing University. A preprint has previously been published (https://doi.org/10.21203/rs.3.rs-2605769/v1) [35].

Conflicts of Interest

The authors declare that they have no conflicts of interest.

Authors' Contributions

Wu Wenjie is mainly responsible for data processing and paper writing. Thanks to Yilei Gu and Xiaopeng Su for their help during the experiment. Thank Yilei Gu and Chee-Ming Chan for their constructive comments, which helped to improve the quality of the paper.

Acknowledgments

This work is supported by the Natural Science Foundation Project of Chongqing (no. cstc2021jcyj-msxmX0929) and Fujian Forestry Vocational & Technical College (no. 2023BK04).

References

[1] M. F. Cai, M. C. He, and D. Y. Liu, *Rock Mechanics and Engineering*, Science Press, Beijing, 2002.

[2] Z. Liu, "Damage constitutive of cyclic loading and damage threshold of rock under high confining pressure," *Chinese Journal of High Pressure Physics*, vol. 34, no. 4, pp. 108–116, 2020.

[3] J. Kim, J. Yi, J. Kim, G. Zi, and J. S. Kong, "Fatigue life prediction methodology using entropy index of stress interaction and crack severity index of effective stress," *International Journal of Damage Mechanics*, vol. 22, no. 3, pp. 375–392, 2013.

[4] C. Zhang and Y. Bai, "Establishment and application of parametric geometrical damage model of rocks," *Rock and Soil Mechanics*, vol. 41, no. 12, pp. 3899–3909, 2020.

[5] C. Wang, S.-F. Zhan, M.-Z. Xie, C. Wang, L.-P. Cheng, and Z.-Q. Xiong, "Damage characteristics and constitutive model of deep rock under frequent impact disturbances in the process of unloading high static stress," *Complexity*, vol. 2020, Article ID 2706091, 15 pages, 2020.

[6] J. S. O. Lau and N. A. Chandler, "Innovative laboratory testing," *International Journal of Rock Mechanics and Mining Sciences*, vol. 41, no. 8, pp. 1427–1445, 2004.

[7] K. Huang, F. Zha, B. Kang, X. Sun, and J. Su, "An energy-based damage model for red-bed sandstones subjected to drying–wetting cycles," *Geotechnique Letters*, vol. 11, no. 3, pp. 215–220, 2021.

[8] X. Wang, Z. Wen, Y. Jiang, and H. Huang, "Experimental study on mechanical and acoustic emission characteristics of rock-like material under non-uniformly distributed loads," *Rock Mechanics and Rock Engineering*, vol. 51, no. 3, pp. 729–745, 2018.

[9] M. Naderloo, M. Moosavi, and M. Ahmadi, "Using acoustic emission technique to monitor damage progress around joints in brittle materials," *Theoretical and Applied Fracture Mechanics*, vol. 104, Article ID 102368, 2019.

[10] N. Yousefpour and M. Pouragha, "Prediction of the post-failure behavior of rocks: combining artificial intelligence and acoustic emission sensing," *International Journal for Numerical and Analytical Methods in Geomechanics*, vol. 46, no. 10, pp. 1874–1894, 2022.

[11] Z.-H. Zhang and J.-H. Deng, "A new method for determining the crack classification criterion in acoustic emission parameter analysis," *International Journal of Rock Mechanics and Mining Sciences*, vol. 130, Article ID 104323, 2020.

[12] A. Thirumalaiselvi and S. Sasmal, "Pattern recognition enabled acoustic emission signatures for crack characterization during damage progression in large concrete structures," *Applied Acoustics*, vol. 175, Article ID 107797, 2021.

[13] H. Nazaripoor, H. Ashrafizadeh, R. Schultz, J. Runka, and P. Mertiny, "Acoustic emission damage detection during three-point bend testing of short glass fiber reinforced composite panels: integrity assessment," *Journal of Composites Science*, vol. 6, no. 2, Article ID 48, 2022.

[14] M. De Smedt, E. Vandecruys, R. Vrijdaghs, E. Verstrynge, and L. Vandewalle, "Acoustic emission-based damage analysis of steel fibre reinforced concrete in progressive cyclic uniaxial tension tests," *Construction and Building Materials*, vol. 321, Article ID 126254, 2022.

[15] S. Livadiotis, K. Sitaropoulos, A. Ebrahimkhanlou, and S. Salamone, "Acoustic emission monitoring of corrosion in steel pipes using Lamb-type helical waves," *Structural Health Monitoring*, vol. 22, no. 2, pp. 1225–1236, 2023.

[16] L. B. Andraju and G. Raju, "Damage characterization of CFRP laminates using acoustic emission and digital image correlation: clustering, damage identification and classification," *Engineering Fracture Mechanics*, vol. 277, Article ID 108993, 2023.

[17] Q. Siqing, *An Introduction to Acoustic Emission Techniques in Rocks*, Southwest Jiaotong University Press, Chengdu, 1993.

[18] A. Muñoz-Ibáñez, J. Delgado-Martín, M. Herbón-Penabad, and J. Alvarellos-Iglesias, "Acoustic emission monitoring of mode I fracture toughness tests on sandstone rocks," *Journal of Petroleum Science and Engineering*, vol. 205, Article ID 108906, 2021.

[19] S.-H. Chang and C.-I. Lee, "Estimation of cracking and damage mechanisms in rock under triaxial compression by moment tensor analysis of acoustic emission," *International Journal of Rock Mechanics and Mining Sciences*, vol. 41, no. 7, pp. 1069–1086, 2004.

[20] M. Shigeishi and M. Ohtsu, "Acoustic emission moment tensor analysis: development for crack identification in concrete materials," *Construction and Building Materials*, vol. 15, no. 5-6, pp. 311–319, 2001.

[21] N. N. Sirdesai, T. Gupta, T. N. Singh, and P. G. Ranjith, "Studying the acoustic emission response of an Indian monumental sandstone under varying temperatures and strains," *Construction and Building Materials*, vol. 168, pp. 346–361, 2018.

[22] R. Tripathi, M. Srivastava, S. Hloch, P. Adamčík, S. Chattopadhyaya, and A. K. Das, "Monitoring of acoustic emission during the disintegration of rock," *Procedia Engineering*, vol. 149, pp. 481–488, 2016.

[23] V. L. Shkuratnik, Y. L. Filimonov, and S. V. Kuchurin, "Regularities of acoustic emission in coal samples under triaxial compression," *Journal of Mining Science*, vol. 41, no. 1, pp. 44–52, 2005.

[24] B. X. Liu, J. L. Huang, Z. Y. Wang, and L. Liu, "Study on damage evolution and acoustic emission character of coal–rock under uniaxial compression," *Chinese Journal of Rock Mechanics and Engineering*, vol. 28, no. S1, pp. 3234–3238, 2009.

[25] Z. A. Moradian, G. Ballivy, P. Rivard, C. Gravel, and B. Rousseau, "Evaluating damage during shear tests of rock joints using acoustic emissions," *International Journal of Rock*

Mechanics and Mining Sciences, vol. 47, no. 4, pp. 590–598, 2010.

[26] Y. Yang, D. Wang, M. Guo, and B. Li, “Study of rock damage characteristics based on acoustic emission tests under triaxial compression,” *Chinese Journal of Rock Mechanics and Engineering*, vol. 33, no. 1, pp. 98–104, 2014.

[27] J. Yu, X. H. Liu, and Q. J. Hao, “Acoustic emission characteristics and damage evolution of coal–rock under different confining pressures,” *Coal Geology & Exploration*, vol. 48, no. 3, pp. 128–136, 2020.

[28] Y. Shen, D. Zhang, R. Wang, J. Li, and Z. Huang, “SBD-K-medoids-based long-term settlement analysis of shield tunnel,” *Transportation Geotechnics*, vol. 42, Article ID 101053, 2023.

[29] A. I. Lawal and S. Kwon, “Application of artificial intelligence to rock mechanics: an overview,” *Journal of Rock Mechanics and Geotechnical Engineering*, vol. 13, no. 1, pp. 248–266, 2021.

[30] C. E. Fairhurst and J. A. Hudson, “Draft ISRM suggested method for the complete stress–strain curve for intact rock in uniaxial compression,” *International Journal of Rock Mechanics and Mining Sciences*, vol. 36, no. 3, pp. 279–289, 1999.

[31] J. Lemaitre, “How to use damage mechanics,” *Nuclear Engineering and Design*, vol. 80, no. 2, pp. 233–245, 1984.

[32] X. W. Liu, J. Z. Lin, and Z. Y. Yuan, “Research on evaluation of material fatigue damage by acoustic emission technology,” *China Railway Science*, vol. 18, no. 4, pp. 74–81, 1997.

[33] L. M. Kachanov, “Time of rupture process under creep conditions,” *Izvestiia Akademii Nauk SSSR, Otdelenie Teckhnicheskikh Nauk*, vol. 23, no. 8, pp. 26–31, 1958.

[34] G. Meng, Z. Liu, P. Cao et al., “An initial damage model of rock materials under uniaxial compression considering loading rates,” *Materials*, vol. 15, no. 16, Article ID 5589, 2022.

[35] W. Wu, C. Chan, G. Yilei, and X. Su, “Study on acoustic emission characteristics and damage evolution of shale under uniaxial compression,” *Research Square*, 2023.